Hollow Cathode Electron Beam Formation and Effects on X-Ray Emission in Capillary Discharges

María Pía Valdivia, Edmund S. Wyndham, and Mario Favre

***Abstract*— Electron beams produced by the hollow cathode effect are studied in a compact gas filled 24-kV, 5-kA capillary discharge. The characteristics and role of electron beams on X-ray production are studied in order to better understand their impact on X-ray production. X-ray plasma emission is analyzed with a spectrometer, while wideband diodes and Faraday cup probe both electron beams and X-rays. Electron beams of >5 keV are observed early on the discharge and two types of electron beams are identified: a first beam of high energy and low current (with a speed of $\sim 5 \times 10^7$ m/s and a current density of $\sim 4 \times 10^{-2}$ A/cm^2) enhanced by larger cathode apertures, and a second beam of low energy and high current enhanced by smaller cathode apertures. The use of a simple configuration of external magnets prevents X-ray fluorescence production, caused by electron beams, from reaching electronic detectors hence confusion when evaluating X-ray yield from the plasma source is avoided. This is particularly important in extreme ultraviolet lithography and soft X-ray production applications. Furthermore, the presence of the external magnets does not modify line emission, which is detected by means of spectrometry. Therefore, the use of external magnets provides a way to discriminate X-ray diode signals produced by source emitted X-rays and X-ray fluorescence from electron beams.**

***Index Terms*— Electron emission, gas discharge devices, plasma devices, plasma diagnostics, plasma properties, X-rays.**

I. Introduction

CAPILLARY discharges are utilized for a wide variety of applications, such as high harmonic generation [1], laser waveguides [2], extreme ultraviolet (EUV) lasing and lithography [3], [4], plasma jet generation [5], and soft X-ray lasing and microscopy [6], [7]. The initiation mechanism leading to electric breakdown and subsequent plasma formation along the capillary tube must be chosen according to the application and studies to be undertaken. For soft X-ray and EUV generation, preionization can be employed in order to avoid emission impurities due to wall–plasma interaction, and to favor homogeneous current distribution along the capillary plasma, thus preventing radial expansion. For the configuration discussed here, hollow cathode geometry is used in order to exploit the hollow cathode effect (HCE) as the means of preionization.

Transient hollow cathode discharges are characterized by the presence of an axial aperture in the cathode, which modifies the geometry of the externally applied field to create conditions for local ionization in the hollow cathode region (HCR) before any significant ionization takes place in the anode–cathode gap [8]. The small value of local electric field to gas density ratio in the HCR, compared with the value in the interelectrode space, favors plasma formation by electron impact ionization. The appearance of a hollow cathode plasma leads to the formation of ON-axis electron beams, which allows a sustained electron beam extraction just prior to breakdown, playing an important role in breakdown formation inside the capillary.

The electron beam generation process in transient hollow cathode discharges has been studied for many applications. For example, pseudospark devices have been developed as pulsed power switches [9], EUV radiation sources [10], and as intense electron beam sources [11]. The electron beams produced in the HCR are also applied in material processing [12], thin-film technologies [13], and intense soft X-ray sources [14] in addition to pulsed-electron-beam fluorescence [15] and plasma generation by high energy electron beams, which is one of the most efficient ways of ionizing cold gases [16].

In hollow cathode capillary discharges, two different regimes of electron beams have been reported [17]: 1) a low current high energy beam and 2) a relatively high current beam of low energy. Energetic electron beams with a peak current at the kiloampere level have been reported but the particular conditions under which they are produced was not disclosed [18]. The first intense collimated electron beams generating from the HCR have been reported to have current densities above 10^6 A $\cdot$ cm^{-2} [19]. Similarly, peak current densities higher than 100 A $\cdot$ cm^{-2} have been measured in discharges closer to our geometry [20]. Prebreakdown electron beams are well-centered ON-axis and induce the formation of a fast ionization wave, which propagates axially through the capillary length [8]. The characteristic energy of the electron beams emitted during the high-speed ionization wave propagation can be equal to, but often substantially higher than the energy expected from the applied potential [21], [22]. For the second electron beam, typical currents of around tens of milliamps have been measured [23].

An important characteristic of the discharge is its shot-to-shot reproducibility and potential to high repetition rate, up to the limit of the thermal load to the capillary walls [24]. In our configuration, the mean free path for collisional ionization in the low pressure capillary is of the same order as the capillary length. Hence, the first electron beam pulse does not lead to electric breakdown, which means a substantial flux of high energy electrons is required to

Manuscript received October 2, 2014; revised February 10, 2015; accepted June 10, 2015. Date of publication July 24, 2015; date of current version August 7, 2015. This work was supported by the Fondo Nacional de Desarrollo Científico Tecnológico y de Innovación Tecnológica under Grant 1140950.

The authors are with the Facultad de Física, Pontificia Universidad Católica de Chile, Santiago 7820436, Chile (e-mail: mpvaldivia@pha.jhu.edu).

Color versions of one or more of the figures in this paper are available online at http://ieeexplore.ieee.org.

Digital Object Identifier 10.1109/TPS.2015.2450016

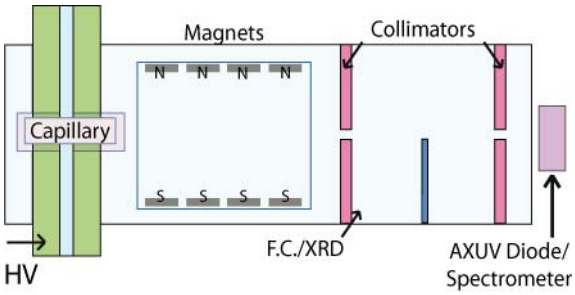

Fig. 1. Diagram of the capillary discharge. X-ray diagnostics and electron bending system.

assist ionization in the capillary volume. It has been reported that the fast electrons shift the ionization equilibrium in the discharge plasma, increasing the emission from the relatively low-temperature plasma [24]–[26], and enhances emission of higher ion species by giving way to a skewed Gaussian temperature distribution [24].

In order to better characterize the role of the electron beams that preionize the gas filled capillary, we probe the hollow cathode electron beams. The effect of these electron beams over the preionization, ionization, and subsequent plasma emission, are discussed. For the first time, we describe a simple method that uses a combination of magnets and collimators to better distinguish the X-ray emission originating from the plasma source and the secondary emission due to electron beam fluorescence.

II. Experimental Details

The constructional details of the discharge have been presented in detail in [27]. The pulsed capillary discharge apparatus uses a 1.6-nF capacitor as energy storage and flowing water serves both as coolant and dielectric. The charging circuit delivers ~0.5 J directly to the capacitor plates in less than 1 μs. The discharge takes place inside an alumina capillary of 21-mm length and 1.6-mm inner diameter. The gas mixture is fed through the cathode and pumped through the anode, thus maintaining a constant flow of nitrogen and helium in a ratio of 10:1, with cathode and anode pressures of 580 and 16 mtorr, respectively. Maximum voltages of 24 kV are used at a repetition rate of 75-Hz. The voltage across the capacitor plates is measured by an external resistive compensated monitor and the current is measured by a single groove Rogowski coil. The diagnostics, shown in Fig. 1, are placed on the anode side, which is at ground potential. They consist of negatively biased Faraday cups (F.C.) detecting both electrons and X-rays, filtered wideband planar diodes, and a time integrated EUV spectrometer covering the range of ~30–400 Å.

The F.C. consists of two gold plated central pins of standard SubMiniature version A connectors connected to solid coaxial cable. They have an effective area of 8 mm^2. A negative going signal corresponds to electron impact and a positive signal to photoelectric emission. The application of negative bias to the pin allows some distinction of energy of the electrons. Although very simple, this implementation provides useful qualitative and some quantitative information. An obvious restriction is that the temporal separation between the impinging electrons and EUV photons. In this experiment,

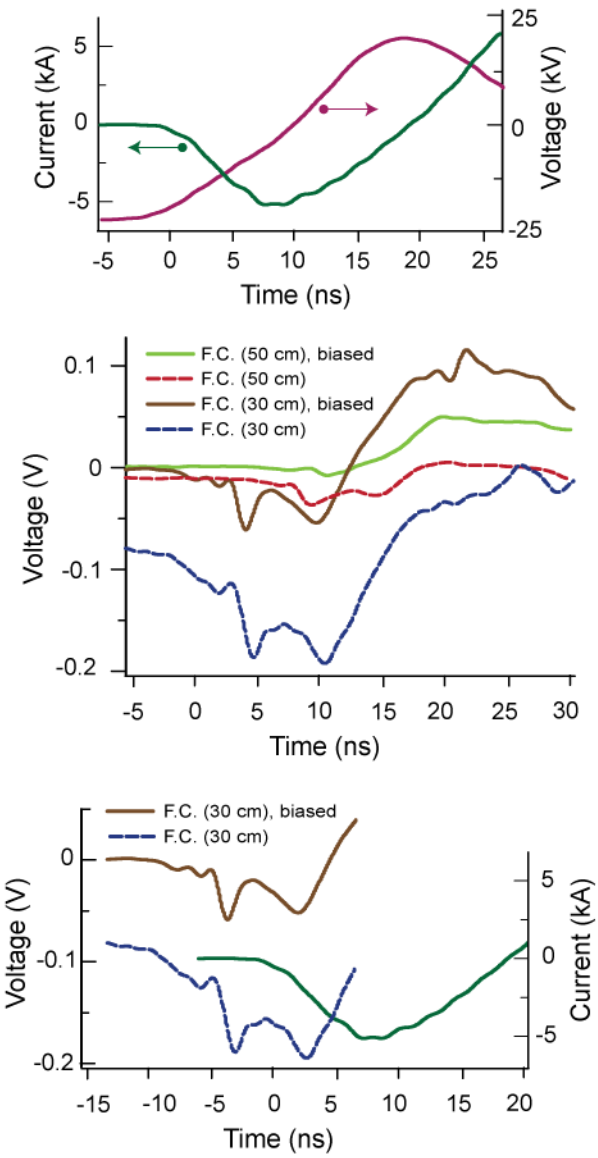

Fig. 2. Top: current and voltage traces for nitrogen discharges. Middle: F.C. signals at two axial positions. Negative going signals originate from electron beams and positive going signals are photoelectric signals from X-rays. Bottom: the portion of the electron beam signal emitted from the anode, corrected for time of flight.

filtered photodiodes show that no significant EUV-soft X-ray emission occurs until 10 ns into the discharge, however, vacuum ultraviolet emission, sufficient to remove photoelectrons from gold, will be generated earlier in the discharge.

III. Experimental Results and Discussion

A combination of F.C. and collimators delivers important information regarding the fast electrons produced by the HCR emerging from the anode aperture. By placing small area cups at two distances, we are able to estimate the energy from time-of-flight measurements. Fig. 2(a) shows the discharge current together with the applied voltage. Fig. 2(b) shows the F.C. signals at two distances, with and without a negative bias of 200 V applied. Fig. 2(c) shows the electron signal corrected for time of flight from the anode exit to the F.C. at 30 cm. Time-of-flight calculations deliver an upper limit for electron beam energy whereas lower energy electron beams

are challenging to measure as they may be overshadowed by signals corresponding to higher energy electrons. An electron beam velocity of $4.1 \pm 0.1 \times 10^7$ m/s and energy of 4.7 ± 0.1 keV are obtained. These values are used in Fig. 2(c) to allow a better estimate of the evolution of the electron beams. Both the biased and unbiased F.C. traces show bursts of electron beam activity leading up to breakdown. It is the final or second electron beam that is associated with full conduction of the capillary [8]. From the voltage trace, we see that there is still a multikilovoltage potential across the capillary at this instant. There are minimal differences in the form of these pulses between the biased and unbiased probes, merely an effect on their amplitude.

A means of estimating the overall loss of energy in the formation of the beams, inner wall surface current, and ionization during the prebreakdown period may be made by comparing the charging voltage with and without a filling gas. A difference of 30% in the stored voltage is observed. On using a SPICE [28] simulation of the charging circuit, we find that the observed charging voltage may be simulated by including a 600-Ω resistor as the equivalent of the capillary before breakdown. We expect the equivalent load of the capillary to be nonlinear. However, even in the over simplistic case of a constant 600-Ω load, the power prior to breakdown reaches 1 MW.

A filtered Si diode may also be used to detect beam target radiation. This has the advantage that the beam and EUV components may be separated using magnets to bend the beam away from the detector. A combination of bending magnets and collimators was installed in order to avoid confusion between X-ray radiation from the plasma source and X-ray fluorescence (from electron beams impacting surfaces along their path) reaching the diode. The diode is filtered with 1.5-μm aluminum, which allows the observation of radiation at longer wavelengths of ~170–70 Å, which is known to be predominant, as observed from spectroscopic studies reported elsewhere [25]. However, only electrons with energy greater than the Kα edge (~1.5 keV) will give a significant X-ray yield that will penetrate the filter to arrive at the diode. This set of observations is shown in Fig. 3. In addition, we present traces for two different Hollow Cathode apertures: 0.7 and 1.5 mm. The evolution of the electron beam pulses depends notably on the aperture diameter. The traces are referenced in time to the current trace [Fig. 3(a)]. Electron beam activity is shown from 30 ns before breakdown to 40 ns afterward. We show four combinations of collimation and bending magnets (including their complete absence). The four combinations are: 1) bending magnets and collimators [Fig. 3(b)]; 2) bending magnets only [Fig. 3(c)]; 3) open path [Fig. 3(d)]; and 4) collimators only [Fig. 3(e)]. The time axis refers to the observed Si diode signals at 60 cm from the anode. This means that the e-beams originate approximately 15 ns earlier, assuming the value obtained from Fig. 2.

In Fig. 3(b) (magnets + collimators), we only observe line-of-sight EUV/soft X-rays. Here, we find a modest X-ray signal for both cathode apertures starting at about 10 ns. It is at this time that we see He-like nitrogen emission as

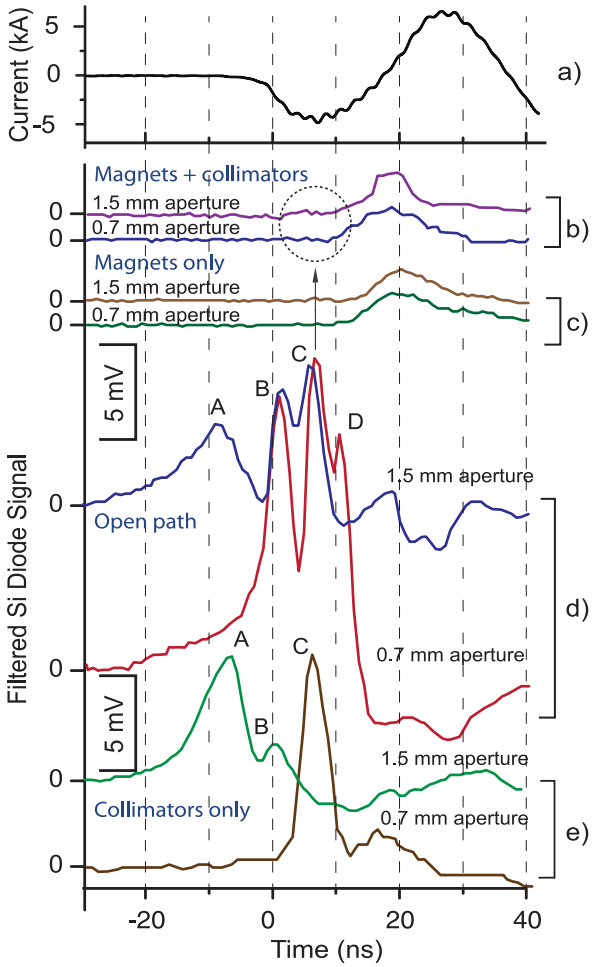

Fig. 3. Nitrogen discharges with a cathode diameter of 0.7 and 1.5 mm. (a) Current. Diode signals corresponding to four data acquisition configurations. (b) Magnets + collimators. (c) Magnets. (d) Open path. (e) Collimators.

reported in [24], which is also observed when the bending magnets are present [Fig. 3(c)]. Upon removal of bending magnets [Fig. 3(d) and (e)], the X-ray signals detected by the diode show additional peaks, which are of such intensity that, along with the reflection due to the electrical mismatch, they completely wash out the expected X-ray signal featured in Fig. 3(b) and (c).

The effect of fluorescence and the hollow cathode aperture diameter becomes apparent in Fig. 3(d) and (e). The signals for both cathode apertures in Fig. 3(d) and (e) show significant intensity well before current rise. It should be noted that the 1.5-mm cathode aperture diameter is essentially that of the capillary and the anode exit aperture. The traces corresponding to the 1.5-mm cathode aperture show a first peak (A). This is not observed for the 0.7-mm aperture. Given that this peak is only present in the larger cathode aperture configuration, it is thus attributed to early noncollimated electron beams producing X-ray fluorescence that reaches the diode. Hence, the production of more collimated electrons in the 0.7-mm cathode aperture geometry would explain the absence of peak A. In particular, Fig. 3(d) shows two sequential peaks (B and C) that are present for both cathode apertures. The 0.7-mm cathode aperture signal also shows a third sequential peak (D) not observed for the

1.5-mm cathode aperture. When the path includes the collimators [Fig. 3(e)], the double peaks B and C, observed in Fig. 3(d), change to a single peak (B) of lower intensity using collimation. Peak B shown in Fig. 3(d) is larger than in Fig. 3(e) (with collimators in place) and it is only present in the 1.5-mm cathode diameter case. This peak is thought to be due to less collimated electrons, in analogy to the previous argument for peak A. Therefore, peak B must come from the so-called second electron beam, which is associated with full conduction. The collimation of this second electron beam is expected to be better for cathode apertures of 0.7 mm.

Peak C is only present for the 0.7-mm cathode diameter, which is explained by higher energy collimated electrons reaching the diode detector. This is corroborated on taking their estimated energies into account. Given the high energy of these electrons (kiloelectronvolt order), peak C is observed [Fig. 3(b)] as a small signal before current maximum is reached. Similarly, peak D is attributed to the second and more collimated electron beam reaching the detector surface, which is corroborated by the absence of this peak in the 1.5-mm cathode diameter signal. In contrast, peak A is attributed to the effect of electrons distributing as a cone rather than a straight line. As mentioned previously, these electrons produce X-ray fluorescence that is detected by the diode.

We summarize the complex morphology of Fig. 3 as follows: peak A is due to fluorescence of the first electron beam. Peaks B–D are due to the second electron beam. Peak B is attributed to X-ray from surface fluorescence, while peaks C and D are due to detector surface interaction of highly collimated and less collimated beams, respectively. The most interesting point is that the electron collimation strongly depends on the cathode aperture, where smaller apertures enhance collimation.

In a previous publication, the effect of changing the cathode diameter was explored and found to affect the duration of the electron beams before breakdown [29]. In these studies, we observed that the small cathode diameter enhances electron beam generation in the HCR for the second beam. This has been observed to enhance emission in the low energy X-ray range (∼200–800 Å). On the other hand, the large aperture enhances the electron beam production of the first electron beam, which in turn increases higher energy X-ray emission [24], [25], [27]. The existence of two different electron beams [17] supports the description of diode signals in the absence of bending magnets and/or collimators. The electrons are able to reach the detector and/or produce X-ray fluorescence when impacting a surface in their path. Hence, it is important to consider these effects when measuring energy output and analyzing X-ray emission.

The X-ray spectrum was analyzed in order to determine the effect of electron beams on the observed emission for nitrogen discharges. Spectra corresponding to a nitrogen capillary discharge (Fig. 4) show line emission with and without external magnets. It can be seen that there is little difference in line emission characteristics when electron beams are allowed to reach the spectrometer. However, a significant background radiation is observed when the magnets are removed, but it does not originate any additional line radiation, thus showing

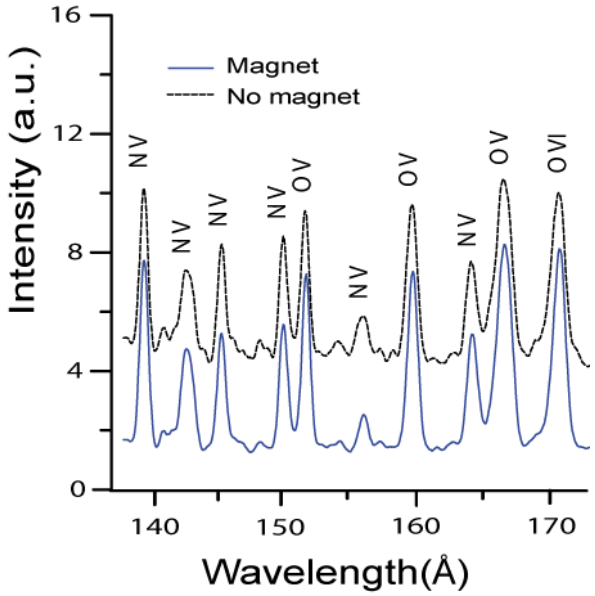

Fig. 4. Nitrogen spectra corresponding to configurations with and without magnets.

X-ray fluorescence from electron beams is polychromatic in nature. The emission lines themselves and their relative intensities are unaffected by both the presence of external magnets deviating electron beams outside the capillary and the fluorescence X-rays produced by these electron beams. This may be important in correcting errors in the so-called Flying Circus measurement of 13.5-nm output for lithography [30].

IV. Summary

As discussed, the confusion between fluorescence and source produced X-rays can be avoided using a simple combination of magnets and collimators, which bend the trajectory of electron beams and prevent fluorescence X-rays from reaching the diagnostics. This is especially relevant in soft X-ray and EUV generation applications since the measurement of in-band energy might result in erroneous measurements when electron beams impact surfaces causing fluorescence at a variety of wavelengths (as seen in our results) due to the high electron beam energies achieved in capillary discharges. However, the spectral results show that the emission lines and their relative intensities are not altered by electron beams and fluorescence, since only a low background radiation, due to X-ray fluorescence, is observed when utilizing a monochromator scheme. Thus, electron beams and the consequent X-ray fluorescence do not affect the proper interpretation of spectral results, unlike electronic diagnostic results. It was also found that 1.5-mm cathode apertures enhance the production of the first electron beam which is of high energy [29], but this is associated with the undesirable result of low average degree of ionization as measured in the relative intensity of N VI emission [25]. Conversely, 0.7-mm cathode apertures enhance the second electron beam of lower energy and are associated with higher ionization [24], [25], [27].

REFERENCES

[1] B. A. Reagan *et al.*, "Enhanced high-order harmonic generation from Xe, Kr, and Ar in a capillary discharge," *Phys. Rev. A*, vol. 76, p. 013816, Jul. 2007.

[2] A. Butler, D. J. Spence, and S. M. Hooker, "Guiding of high-intensity laser pulses with a hydrogen-filled capillary discharge waveguide," *Phys. Rev. Lett.*, vol. 89, p. 185003, Oct. 2002.

[3] M. A. Klosner and W. T. Silfvast, "Intense xenon capillary discharge extreme-ultraviolet source in the 10–16-nm-wavelength region," *Opt. Lett.*, vol. 23, no. 20, pp. 1609–1611, 1998.

[4] Z. Andreic, S. S. Ellwi, S. Pleslic, and H.-J. Kunze, "Performance of the 13.5 nm PVC capillary discharge EUV source," *Phys. Lett. A*, vol. 335, nos. 5–6, pp. 430–434, 2005.

[5] L. S. Caballero, H. Chuaqui, M. Favre, I. Mitchell, and E. Wyndham, "Plasma jet emission in fast-pulsed capillary discharges," *J. Appl. Phys.*, vol. 98, no. 2, p. 023305, 2005.

[6] J. J. Rocca, V. Shlyaptsev, F. G. Tomasel, O. D. Cortazar, D. Hartshorn, and J. L. A. Chilla, "Demonstration of a discharge pumped table-top soft-X-ray laser," *Phys. Rev. Lett.*, vol. 73, pp. 2192–2195, Oct. 1994.

[7] P. Vrba, S. V. Zakharov, A. Jancarek, M. Vrbova, M. Nevrkla, and P. Kolar, "Pinching capillary discharge as a water window radiation source," *J. Electron Spectrosc. Rel. Phenomena*, vol. 184, nos. 3–6, pp. 335–337, 2011.

[8] M. Favre, P. Choi, H. Chuaqui, I. Mitchell, E. Wyndham, and A. M. Lenero, "Experimental investigation of ionization growth in the pre-breakdown phase of fast pulsed capillary discharges," *Plasma Sour. Sci. Technol.*, vol. 12, no. 1, pp. 78–84, 2003.

[9] K. Bergmann, R. Lebert, J. Kiefer, and W. Neff, "Triggering a radial multichannel pseudospark switch using electrons emitted from material with high dielectric constant," *Appl. Phys. Lett.*, vol. 71, no. 14, pp. 1936–1938, 1997.

[10] E. Dewald, K. Frank, D. H. H. Hoffmann, and A. Tauschwitz, "Plasma development in the low-pressure channel spark for pulsed intense electron beam generation," *IEEE Trans. Plasma Sci.*, vol. 30, no. 1, pp. 363–374, Feb. 2002.

[11] H. Yin *et al.*, "Millimeter wave generation from a pseudospark-sourced electron beam," *Phys. Plasmas*, vol. 16, no. 6, p. 063105, 2009.

[12] E. Dewald *et al.*, "Pulsed intense electron beams generated in transient hollow cathode discharges: Fundamentals and applications," *IEEE Trans. Plasma Sci.*, vol. 25, no. 2, pp. 272–278, Apr. 1997.

[13] T. Witke, A. Lenk, and P. Siemroth, "Channel spark discharges for thin film technology," *IEEE Trans. Plasma Sci.*, vol. 25, no. 4, pp. 758–762, Aug. 1997.

[14] O. Rosier *et al.*, "Frequency scaling in a hollow-cathode-triggered pinch plasma as radiation source in the extreme ultraviolet," *IEEE Trans. Plasma Sci.*, vol. 32, no. 1, pp. 240–246, Feb. 2004.

[15] F. M. Lufty and E. P. Muntz, "Initial experimental study of pulsed electron beam fluorescence," *AIAA J.*, vol. 34, no. 3, pp. 478–482, 1996.

[16] S. O. Macheret, M. N. Shneider, R. B. Miles, and R. J. Lipinski, "Electron-beam-generated plasmas in hypersonic magnetohydrodynamic channels," *AIAA J.*, vol. 39, no. 6, pp. 1127–1138, 2001.

[17] P. Choi, H. H. Chuaqui, M. Favre, and E. S. Wyndham, "An observation of energetic electron beams in low-pressure linear discharges," *IEEE Trans. Plasma Sci.*, vol. 15, no. 4, pp. 428–433, Aug. 1987.

[18] D. Bloess *et al.*, "The triggered pseudo-spark chamber as a fast switch and as a high-intensity beam source," *Nucl. Instrum. Methods Phys. Res.*, vol. 205, nos. 1–2, pp. 173–184, Jan. 1983.

[19] J. Christiansen and C. Schultheiss, "Production of high current particle beams by low pressure spark discharges," *Zeitschrift Phys. A, Atoms Nucl.*, vol. 290, no. 1, pp. 35–41, 1979.

[20] M. Favre, H. Chuaqui, E. S. Wyndham, and P. Choi, "Measurements on electron beams in pulsed hollow-cathode discharges," *IEEE Trans. Plasma Sci.*, vol. 20, no. 2, pp. 53–56, Apr. 1992.

[21] W. Benker *et al.*, "Generation of intense pulsed electron beams by the pseudospark discharge," *IEEE Trans. Plasma Sci.*, vol. 17, no. 5, pp. 754–757, Oct. 1989.

[22] G. Avaria *et al.*, "Hollow cathode effects in the pre-breakdown phase of a pulsed capillary discharge," *Plasma Sour. Sci. Technol.*, vol. 18, no. 4, p. 045014, 2009.

[23] P. Choi and M. Favre, "Fast pulsed hollow cathode capillary discharge device," *Rev. Sci. Instrum.*, vol. 69, no. 9, p. 3118, 1998.

[24] M. P. Valdivia, E. S. Wyndham, E. Ramos-Moore, P. Ferrari, and M. Favre, "Observations of soft X-ray emission and wall ablation in a fast low-energy pulsed capillary discharge," *J. Phys. D, Appl. Phys.*, vol. 46, no. 31, p. 315201, 2013.

[25] M. P. Valdivia, E. S. Wyndham, M. Favre, J. C. Valenzuela, H. Chuaqui, and H. Bhuyan, "Observations of the emission processes of a fast capillary discharge operated in nitrogen," *Plasma Sour. Sci. Technol.*, vol. 21, no. 2, p. 025011, 2012.

[26] S. V. Zakharov, V. S. Zakharov, V. G. Novikov, M. Mond, and P. Choi, "Plasma dynamics in a hollow cathode triggered discharge with the influence of fast electrons on ionization phenomena and EUV emission," *Plasma Sour. Sci. Technol.*, vol. 17, no. 2, p. 024017, 2008.

[27] E. S. Wyndham, M. Favre, M. P. Valdivia, J. C. Valenzuela, H. Chuaqui, and H. Bhuyan, "Fast plasma discharge capillary design as a high power throughput soft X-ray emission source," *Rev. Sci. Instrum.*, vol. 81, no. 9, p. 093502, 2010.

[28] *LTspice [CD-ROM]*, Linear Technol., Milpitas, CA, USA, 2015. [Online]. Available: http://www.linear.com/

[29] M. Favre *et al.*, "Hollow cathode effects in charge development processes in transient hollow cathode discharges," *IEEE Trans. Plasma Sci.*, vol. 23, no. 3, pp. 212–220, Jun. 1995.

[30] R. Stuik *et al.*, "Portable diagnostics for EUV light sources," in *Proc. Int. Symp. Opt. Sci. Technol.*, 2000, pp. 121–127.

María Pía Valdivia was born in Santiago, Chile. She received the Ph.D. degree from the Pontificia Universidad Católica de Chile, Santiago, in 2011.

She has been involved in experimental research with the Department of Physics and Astronomy, Johns Hopkins University, Baltimore, MD, USA, since 2013, where she has participated in the construction and development of high-energy-density (HED) X-ray diagnostics as a Post-Doctoral Researcher. Her current research interests include the investigation of HED physics topics, such as laser-produced plasmas, fast transient plasmas, plasmas generated using high currents, and general plasma diagnostics.

Edmund S. Wyndham was born in U.K. He received the Ph.D. degree in problems of nonlinear heat flux in plasmas from Imperial College London, University of London, London, U.K., in 1982.

He has been involved in experimental research with the Pontificia Universidad Católica de Chile, Santiago, Chile, since 1983, where he has participated in the construction and development of the Plasma Laboratory Research Facility.

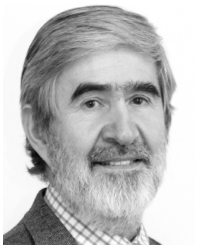

Mario Favre was born in Santiago, Chile. He received the B.Sc. degree from the Pontificia Universidad Católica de Chile, Santiago, in 1980, and the Ph.D. degree from Imperial College London, London, U.K., in 1985.

He has been with the Plasma Physics Group, Institute of Physics, Pontificia Universidad Católica de Chile, Santiago, since 1985. His current research interests include fast transient plasmas, including pulsed capillary discharges, wire array and exploding wire discharges and laser produced plasmas, and plasma-based techniques for thin-film deposition.